

Level Set Modeling of Transient Electromigration Grooving *

M. Khenner¹ A. Averbuch¹ M. Israeli² M. Nathan³ E. Glickman³

¹Department of Computer Science
School of Mathematical Sciences
Tel Aviv University, Tel Aviv 69978, Israel

² Faculty of Computer Science
Technion, Haifa 32000, Israel

³Department of Electrical Engineering-Physical Electronics
Faculty of Engineering
Tel Aviv University, Tel Aviv 69978, Israel

Abstract

A numerical investigation of grain-boundary (GB) grooving by means of the Level Set (LS) method is carried out. GB grooving is emerging as a key element of electromigration drift in polycrystalline microelectronic interconnects, as evidenced by a number of recent studies. The purpose of the present study is to provide an efficient numerical simulation, allowing a parametric study of the effect of key physical parameters (GB and surface diffusivities, grain size, current density, etc) on the electromigration drift velocity as well as on the morphology of the affected regions. An idealized polycrystalline interconnect which consists of grains separated by parallel GBs aligned normal to the average orientation of interconnect's surface is considered. Surface and grain-boundary diffusion are the only diffusion mechanisms assumed. The diffusion is driven by surface curvature gradients and by an externally applied electric field. The corresponding mathematical system is an initial boundary value problem for a two-dimensional Hamilton-Jacobi type equation. To solve for the electrostatic problem at a given time step, a full model based on the solution of Laplace's equation for the electric potential is employed. The resulting set of linear algebraic equations (from the finite difference discretization of the equation) is solved with an effective multigrid

*This research was supported by the Israeli Ministry of Science and Technology grant #9672-1-96 - 9672-3-98.

iterative procedure. The details of transient slit and ridge formation processes are presented and compared with theoretical predictions on steady-state grooving [1, 2, 3].

Keywords: Level Set method, modeling, electromigration, grain boundary grooving, drift.

1 Introduction

This paper is a continuation of our work on numerical modeling of the formation and propagation of groove-like defects at GBs in thin film polycrystalline interconnects used in microelectronics (ME).

In modern ME industry, the reliability of ME integrated circuits has become no less important than their performance. Some of the most vulnerable elements of ME circuits, susceptible to several types of failures, are the interconnects. These are thin film metallic conductors which connect the active elements.

The defects (due to the small cross-section, high current density, mechanical stresses and presence of GBs acting as fast diffusion pathways) lead to a loss (in relatively short times) of electrical and mechanical integrity, i.e. to line opens or shorts. For example, in the presence of a large GB flux ($J_{gb} \approx 10^{-4} \mu\text{m}^2/\text{s}$) a groove can extend several micrometers in a few hours [2]. Thus, GB grooving is one of the main failure mechanisms in advanced integrated circuits.

In the absence of an external potential field and mechanical stresses, the GB atomic flux $J_{gb} = 0$, and the corresponding groove profile evolves via surface diffusion under well-known conditions of scale and temperature (the so-called Mullins problem [4]). In this case, mass transport by surface diffusion is driven only by the surface Laplacian of curvature. Essentially, matter flows from low-curvature regions to high-curvature regions.

In [5], we presented and discussed the numerical approach (e.g. the Level Set (LS) method) used to model GB grooving phenomena. We also tested the LS method on two simple, already solved, grooving problems: Mullins problem, and that of GB grooving by surface diffusion in a periodic array of stationary GBs [6]. In both cases, the results obtained by means of the LS method are in good agreement with the theoretical predictions. In this paper, we consider the second geometry only, as being more realistic (see Fig. 1). Due to axial symmetry at $x = 0, x = L$ (where L is the grain size), we do not attempt to calculate groove branches at $x < 0, x > L$.

Electric fields/currents in metallic conductors provide an additional driving force for surface/GB mass fluxes [7]. In the presence of an electric field, collisions between the conduction electrons and the metal ions lead to drift of the ions. This process is known as electromigration (EM).

GB grooving with a GB flux in real thin film interconnects is a complex problem. An adequate numerical modeling technique should be capable to manage such issues as GB grooving with an arbitrary EM flux, and various ratios of GB to surface diffusivities; the latter was predicted to critically affect groove kinetics and shape, and thus account for various EM failure regimes (see [1, 2, 3] and the references therein). In cited works, analytical and semi-analytical approaches for analysing steady-state grooving regimes were employed. However, to our knowledge, no effort has been made to directly

numerically simulate the transient stage during GB grooving. This is the ultimate goal of this paper.

We do not consider mechanical stresses in GBs which, as a matter of fact, are invariably induced by the field [7] (the approximations under which it is reasonable to neglect the stress are discussed in [2, 3]). Also, under typical operational conditions of ME interconnects, lattice transport may be neglected compared to surface/GB transport [8, 9].

Our paper proceeds as follows. In Section 2, we give details of the physical formulation. In Section 3, we discuss some improvements in the numerical algorithm and also the aspects which are due to incorporation of the electric field/GB flux in the model (for other algorithmic details, the interested reader should refer to [5]). Our numerical results and discussion are presented in Section 4.

2 Physical model

2.1 Driving forces for the diffusion

In the absence of an electric current, the surface diffusion is driven by a variation in chemical potential, μ_s , which causes atoms to migrate from high potential to low potential regions. It was shown [4] that

$$\mu_s = K_s \gamma_s \Omega \quad (2.1)$$

where K_s is the surface curvature, γ_s is the surface tension, and Ω is the atomic volume. Gradients of chemical potential are therefore associated with gradients of curvature.

Let τ be the tangential direction to the surface profile in 2D. Let x, y be Cartesian coordinates along horizontal and vertical boundaries of the computational box (Fig. 1). If $\mathbf{n} = (n_x, n_y)$ is the unit vector normal to the surface, then the following relations hold:

$$\tau = (n_y, -n_x), \quad \frac{\partial K_s}{\partial \tau} = \nabla K_s \cdot \tau = \frac{\partial K_s}{\partial x} n_y - \frac{\partial K_s}{\partial y} n_x \equiv K_\tau^s. \quad (2.2)$$

The corresponding surface flux (volume crossing unit length per unit time) is then given by

$$J_s^{\nabla K_s} = -\frac{D_s \delta_s}{kT} \frac{\partial \mu_s}{\partial \tau} = -B K_\tau^s \quad (2.3)$$

where the superscript indicates that the flux is due to the curvature gradient,

$$B = \frac{D_s \delta_s \gamma_s \Omega}{kT} \quad (2.4)$$

is known as Mullins constant, and D_s , δ_s , k , and T denote surface diffusion coefficient, thickness of the surface diffusion layer, Boltzmann's constant and absolute temperature, respectively. Note that $J_s^{\nabla K_s}$ is proportional to the first directional derivative of the curvature.

If an electric field is present, the flux J_s of matter at the curved surface of the conductor is driven simultaneously by curvature gradients, and by the component E of the *local* electric field along the surface. In what follows, we distinguish between two models which handle the electric field:

1. Piecewise-constant electric field

Let C and O denote the conductor (interconnect) material domain and the outer (surrounding) material domain above the surface profile, respectively (see Fig. 1). In this model, the vector of the electric field intensity is parallel to the GBs, $\mathbf{E}_0 = (0, E_{0y})$, and E_{0y} is a step function,

$$E_{0y}(x_i, y_j, t) = \begin{cases} E_0^{in} = \text{const.} & \text{if grid point } (x_i, y_j) \in C \\ E_0^{out} = \text{const.} & \text{if grid point } (x_i, y_j) \in O. \end{cases} \quad (2.5)$$

We assume that the surrounding material is less conductive than the interconnect material, and therefore $|E_0^{out}| < |E_0^{in}|$. In our numerical experiments we chose the ratio $|E_0^{out}|/|E_0^{in}| = 0.1$. In the finite difference approach, the discontinuous distribution of electric field intensity is smoothed out across the surface profile (see the details in Section 3). The component of the *local* electric field along the surface, E , is then approximated by the projection of \mathbf{E}_0 on the surface, $E = \mathbf{E}_0 \cdot \tau$. This approximates the true value given by solving Laplace's equation for the potential, subject to the boundary conditions of constant fields of magnitudes E_0^{in} and E_0^{out} in the conductor and surrounding material domains, respectively.

The corresponding electrically induced surface flux of matter is given by

$$J_s^E = -\frac{D_s \delta_s Z_s}{kT} E = -B_e E \quad (2.6)$$

where the superscript indicates that the flux is due to the electric field, and

$$B_e = \frac{D_s \delta_s Z_s}{kT} \quad (2.7)$$

where $Z_s = z_s^* e$ is the effective charge of the ions undergoing electromigration in the surface layer and e is the unit electronic charge; the sign of z_s is usually positive (i.e., matter flux in the direction of the electron flow).

2. Solution of Laplace's equation for the potential

Assume that (at a given time step of overall marching algorithm) $U(x, y)$ is the electric potential within the (rectangular) computational box. $U^-(U^+)$ and $U^+(U^-)$ are its values on the upper and lower boundaries of the box, and U_n is the normal derivative on the boundary. U^- and U^+ are assumed to be time-independent and uniform along the boundaries; $U^+ - U^-$ is the external voltage applied to the interconnect. The distribution $U(x, y)$ is governed by a static elliptic PDE

$$\frac{\partial}{\partial x} \left(k \frac{\partial U}{\partial x} \right) + \frac{\partial}{\partial y} \left(k \frac{\partial U}{\partial y} \right) = 0, \quad (2.8)$$

with boundary conditions $U_n = U_x = 0$ on the vertical boundaries of the box (which in our case coincide with GBs). Equation (2.8) is derived from the well-posed three dimensional potential problem for the two-layer interconnect. The assumptions and complete derivation for the case of small aspect ratio are presented in [10]. We also give some details in the Appendix. In eq. (2.8), $k = k(x, y)$ is the specific electrical conductivity (at a given time step) of the material which fills the computational box. To solve (2.8), a finite difference scheme was developed and analysed in [10]. The distribution of the specific conductivity in the

physical system under consideration is discontinuous: the conductivity inside the conductor material (domain C , Fig. 1) differs by a finite value from that of the surrounding material (domain O). We assume

$$k = \begin{cases} k_{in} = \text{const.} > 0 & \text{if grid point } (x_i, y_j) \in C \\ k_{out} = \text{const.} > 0 & \text{if grid point } (x_i, y_j) \in O, \end{cases} \quad (2.9)$$

i.e. $k = k(y)$ is a step function. In our numerical experiments we chose the ratio $k_{out}/k_{in} = 0.1$. Since the surface of the conductor evolves in time and space, then to find the time-dependent solution $U(x, y, t)$ we need to solve the static equation (2.8) every time step with k given by (2.9). In order to be able to compute accurately the electric field intensity (which is the derivative of U), the discontinuous distribution of the specific conductivity is smoothed out across the surface profile. The finite difference discretization of (2.8) in the computational domain leads to a set of linear algebraic equations with a sparse banded matrix. This set is solved with an effective multigrid iterative procedure [10]. The solution of the previous time step is used as an initial approximation for the current step which allows fast convergence.

After the potential is established everywhere in the computational domain, the corresponding electrically induced surface flux J_s^E is given by (2.6), where

$$E = -\tau \cdot \nabla U \quad (2.10)$$

To summarize the above discussion, the total flux of matter along the surface is

$$J_s = J_s^{\nabla K} + J_s^E. \quad (2.11)$$

Physically, equation (2.11) says that atoms will diffuse in the direction of the electron flow if the field dominates, but toward the position with the large curvature if the surface energy dominates. This competition between the electric field and the surface energy is essential for the groove dynamics.

The electric field results also in the diffusion of matter along GBs. The diffusion flux along the GB, J_{gb} , is given by

$$J_{gb} = -\frac{D_{gb}\delta_{gb}Z_{gb}}{kT}E \quad (2.12)$$

where D_{gb} , δ_{gb} , $Z_{gb} = z_{gb}^*e > 0$ are the GB diffusion coefficient, thickness and effective ionic charge, respectively, and E is the component of the electric field along the GB.

2.2 Boundary conditions at groove roots

The evolution of the surface is constrained by two conditions imposed locally at groove roots a and b (Fig. 1):

1. Equilibrium angles

The boundary condition is dictated by the local equilibrium between the surface tension, γ_s , and the GB tension, γ_{gb} . In the symmetric case of a GB ($x = 0$)

normal to an original ($y = \text{const.}$) flat surface, the angle of inclination of the right branch of the surface at the groove root with respect to the x axis is [4]

$$\theta_0 = \sin^{-1}(\gamma_{gb}/2\gamma_s) = \text{const.} \quad (2.13)$$

The rapid establishment of the equilibrium angles between the GBs and the surface by atomic migration in the vicinity of the intersections develops some curvature gradients at the adjacent surface, and thus induces surface diffusion fluxes, $J_s^{\nabla K}$, along the groove walls. The directions of the fluxes depend on the sign of the respective surface curvature gradients at the groove groots.

2. Continuity of electrically induced fluxes

The boundary conditions read

$$J_{gb} = 2J_s^E, \quad (2.14)$$

since both branches of the groove act as sinks or sources of matter.

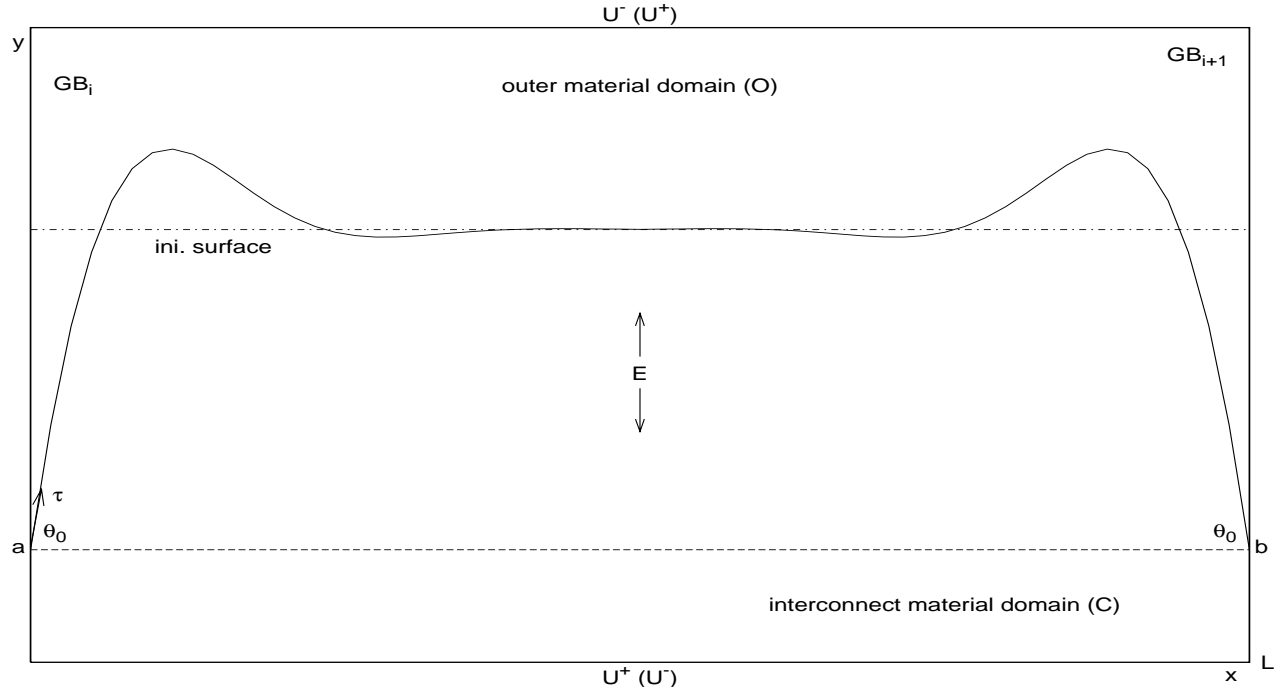


Figure 1: Sketch of GB grooving in a periodic array of stationary GBs. The grain size is L , and groove root points are marked as a and b .

3 The numerical procedure

The Level Set method is used to “capture” the evolution of the conductor surface. The method was introduced by Osher and Sethian [11] and was further developed during the last several years. The method enables to capture drastic changes in the shape of the curves (surfaces or interfaces) and even topology changes.

The basic idea of the method consists of embedding the curve $y(x, t)$ into a higher dimensional space. As a matter of fact, we consider the evolution of a two-dimensional field $\phi(x, y, t)$ such that its zero level set, $\phi(x, y, t) = 0$, coincides with the curve of interest, $y(x, t)$, at any time t . The level set function $\phi(x, y, t)$ can be interpreted as a signed distance from the curve $y(x, t)$, which moves in the direction normal to itself.

The evolution of $\phi(x, y, t)$ is described by an Hamilton-Jacobi type equation. A remarkable trait of the method is that the function $\phi(x, y, t)$ remains smooth, while the level surface $\phi = 0$ may change topology, break, merge, and form sharp corners as ϕ evolves. Thus, it is possible to perform numerical simulations on a discrete grid in the spatial domain, and substitute a finite difference approximations for the spatial and temporal derivatives in time and space. Another nice feature of the method is that the explicit location of the interface needs not to be known in the computational process; all the necessary information is extracted from the level set function.

The evolution equation has the form

$$\phi_t + F|\nabla\phi| = 0 \quad \text{given } \phi(x, t = 0). \quad (3.1)$$

The normal velocity, F , is considered to be a function of spatial derivatives of $\phi(x, y, t)$. In many applications F is a function of the curvature, K_s , and its spatial derivatives. The curvature K_s may be computed via the level set function ϕ as follows:

$$K_s = \nabla \cdot \mathbf{n}, \quad \mathbf{n} = \frac{\nabla\phi}{|\nabla\phi|} = \left(\frac{\phi_x}{(\phi_x^2 + \phi_y^2)^{1/2}}, \frac{\phi_y}{(\phi_x^2 + \phi_y^2)^{1/2}} \right). \quad (3.2)$$

Here \mathbf{n} is a “normal vector”, and it coincides with the (previously introduced) unit normal to the surface, $y(x, t)$, on the zero level set $\phi = 0$. Formulas (3.2) can be combined as follows

$$K_s = \nabla \cdot \frac{\nabla\phi}{|\nabla\phi|} = \frac{\phi_{xx}\phi_y^2 - 2\phi_x\phi_y\phi_{xy} + \phi_{yy}\phi_x^2}{(\phi_x^2 + \phi_y^2)^{3/2}}, \quad (3.3)$$

and the sign of K_s is chosen such that a sphere has a positive mean curvature equal to its radius. In the case of surface diffusion in 2D,

$$F = \frac{\partial J_s}{\partial \tau} = \frac{\partial J_s^{\nabla K}}{\partial \tau} + \frac{\partial J_s^E}{\partial \tau} \quad (3.4)$$

where J_s is given by (2.11).

The difficulties in the numerical solution of (3.1) in our case are due to the fact that, as could be noted from (2.3), (3.3), (3.4), the first term in F contains space derivatives of order 4 of the level set function. Therefore, the evolution equation (3.1) is highly sensitive to errors. Besides, this fourth derivative term leads to schemes with very small time steps.

In [5], we presented the computational algorithm which solves the problem of GB grooving by surface diffusion in the absence of electromigration. This could be viewed as the limiting case of the problem which is under consideration in this paper, corresponding to the situation where electrically induced surface and GBs fluxes J_s^E and J_{gb} vanish. The normal velocity function (3.4) in the latter case contains only the first term. The basic features of the algorithm are:

- the use of a uniform static grid in both space directions
- the use of a standard second order-accurate finite difference scheme in space
- the approximation of spatial derivatives (in normal direction) on the boundaries of the computational box by second order one-sided differences
- time marching is done by a second-order Total Variation Diminishing (TVD) Runge–Kutta procedure [12, 13]
- the use of second-order Essentially Non-Oscillatory (ENO) scheme [14] to approximate the gradient function in (3.1)
- the use of “reinitialization” [15] every time step to keep the level set function ϕ a signed distance function

The solution of (3.1) (in Mullins case of an infinite bicrystal with a single GB) subject to the conditions of a constant angle of surface inclination and zero surface flux $J_s^{\nabla K}$ at the groove root a , is then a self-similar surface profile, whose linear dimensions are proportional to $(Bt)^{1/4}$, B given by (2.4) (Fig. 2). If the dimensions of the crystal are finite, grooves develop at each GB; grooving stops when, at sufficiently long times, identical circular arcs develop connecting adjacent GBs (Fig. 3). The parameters chosen for the runs are typical for copper interconnects at temperatures relevant to experiments ($T = 600$ K) [1, 16]: $\Omega = 1.18 \times 10^{-29}$ m³, $D_s = 3.3 \times 10^{-14}$ m²/s, $\gamma_s = 1.7$ J/m², $\delta_s = 3.5 \times 10^{-10}$ m, $kT = 8.28 \times 10^{-21}$ J. It is worth noting that our numerical treatment of GB grooving is not constrained by the assumption of small equilibrium angles (“small slope approximation”), in contrast to the analytical approaches of the pioneer works [6, 4].

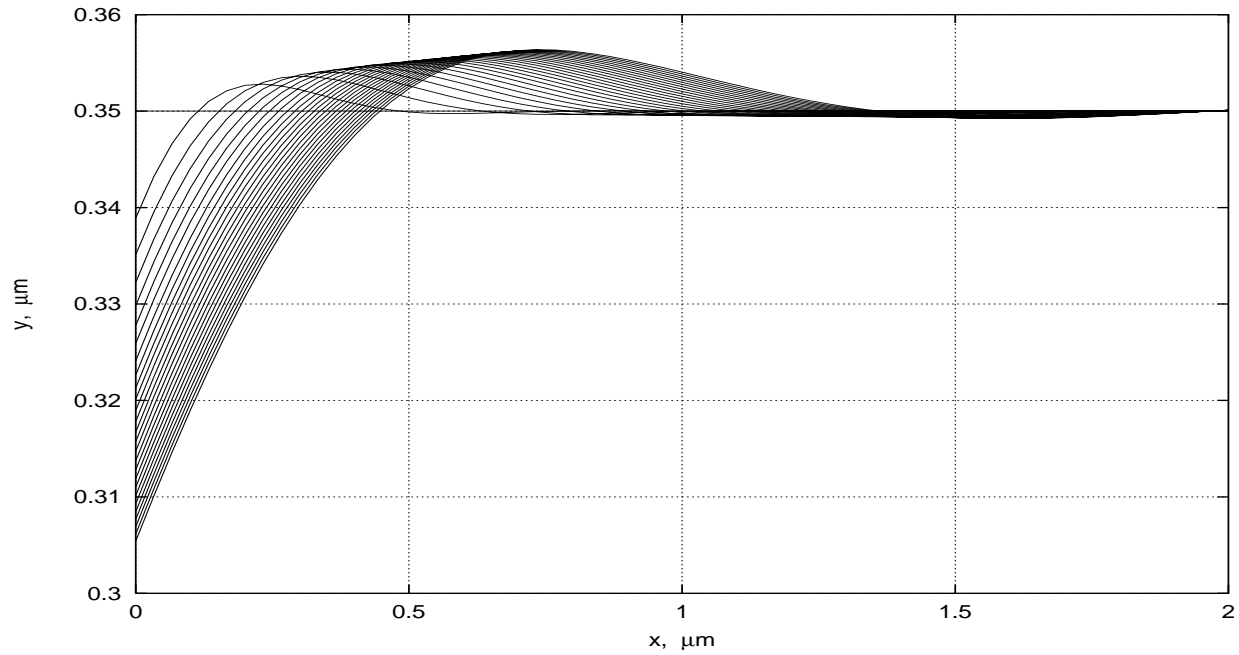


Figure 2: Groove development and propagation along the GB of an infinite bicrystal (Mullins problem). Grain size $L = 2 \mu m$. For copper interconnects at $T = 600 K$ ($327 ^\circ C$), $B = 9.2 \times 10^{-33} m^4/s$. The angle at the groove root $\theta_0 = \pi/22$ ($\tan \theta_0 \approx 0.144$).

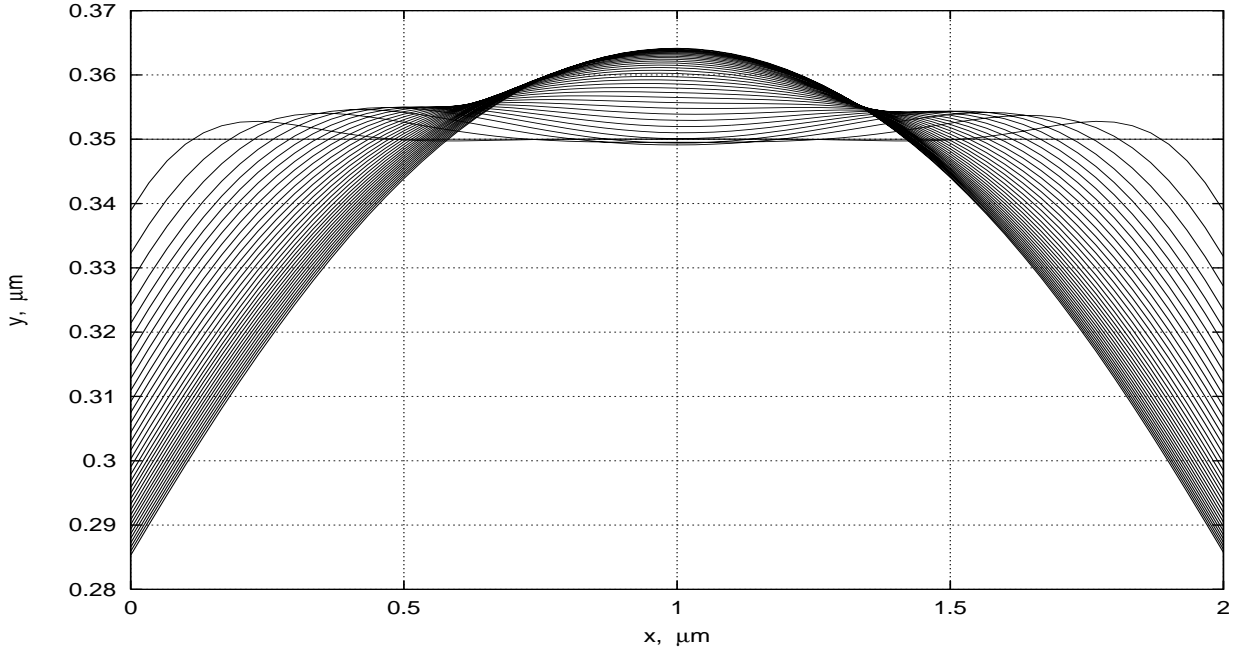


Figure 3: GB grooving in a periodic array of stationary GBs. Parameters are the same as in Fig. 2.

In [5], special attention was given to the treatment of constant-angle and zero-flux conditions at the groove roots within the framework of the Level Set method. Two methods were developed, the first based on interface reconstruction every time step, with subsequent correction of the angles followed with reinitialization, and the second based on the extension of the ϕ -field beyond the GBs using the expansion in Taylor series up to second order. Both methods were successfully used in calculations, but we observed that sometimes both procedures resulted in a loss of accuracy. In this paper, we propose a new, robust and highly accurate procedure to keep the equilibrium angle (2.13) constant at the intersections of the surface with the GBs.

Consider equations (2.2), (3.2) and the zero level line of ϕ (conductor's surface) passing through the groove root point a in Fig. 1 (a similar analysis could be performed for groove root point b). Since the tangential vector to the zero level line at a (as well as to other level lines at $x = 0$ if ϕ is kept a signed distance function), is $\tau = (\cos \theta_0, \sin \theta_0)$, then (2.2), (3.2) imply

$$n_x = -\sin \theta_0 = \frac{\phi_x}{(\phi_x^2 + \phi_y^2)^{1/2}}, \quad n_y = \cos \theta_0 = \frac{\phi_y}{(\phi_x^2 + \phi_y^2)^{1/2}}. \quad (3.5)$$

Dividing the first equation in (3.5) by the second one gives

$$\phi_x = -\phi_y \tan \theta_0. \quad (3.6)$$

As pointed out above, we approximate the spatial derivatives (in normal direction) of ϕ at the boundaries of the computational domain by second order one-sided differences.

Therefore, equation (3.6) written on the left boundary $x = 0$ takes the form

$$\frac{-3\phi_{0,j} + 4\phi_{1,j} - \phi_{2,j}}{2\Delta x} = -\frac{\phi_{0,j+1} - \phi_{0,j-1}}{2\Delta y} \tan \theta_0, \quad j = 0, \dots, m-1 \quad (3.7)$$

where m is the number of grid points in the vertical direction, and Δx and Δy are grid spacings in the horizontal and vertical directions, respectively. Rearranging the terms in (3.7) gives the following set of nonhomogeneous linear algebraic equations with a tridiagonal matrix for unknowns $\phi_{0,j}$, $j = 0, \dots, m-1$:

$$-\frac{\tan \theta_0}{2\Delta y} \phi_{0,j-1} - \frac{3}{2\Delta x} \phi_{0,j} + \frac{\tan \theta_0}{2\Delta y} \phi_{0,j+1} = -\frac{4\phi_{1,j} - \phi_{2,j}}{2\Delta x}. \quad (3.8)$$

The solution to this (and to the similar set at $x = L$) is easily and accurately found at the beginning of every stage of a Runge–Kutta time marching, thus providing the field ϕ which incorporates the correct equilibrium angles at the groove roots.

The described procedure allows us to have a straight horizontal line

$$y(x, 0) = \text{const.} \quad (3.9)$$

where $\text{const.} > 0$ gives the initial height of the material domain, as initial condition for LS simulations. Note that initial condition (3.9) does not match the boundary condition (2.13). This implies that a singularity exists at $x = 0, x = L$ at $t = 0$. This singularity does not present a barrier in solving the system numerically when we select an appropriate numerical scheme. Physically, the equilibrium angle is formed instantaneously compared with the time needed for the evolution of the surface. We are not concerned with the details of this instance. We could use an initial surface which is consistent with the boundary conditions (as done in [5] where Mullins profile served as an initial condition, and we followed the evolution of this profile in time). However, the choice of initial condition (3.9) is more physical.

To close this section, we present the details of the calculation of the normal velocity function (3.4):

1. Calculate curvature induced flux $J_s^{\nabla K_s}$ from (2.3). It is nonzero even at the first time step, since the equilibrium angles (2.13) are formed instantly
2. Calculate the first term in (3.4) by applying the formula

$$\frac{\partial J_s^{\nabla K}}{\partial \tau} = \nabla \left[\nabla J_s^{\nabla K} \cdot \tau \right] \cdot \tau = \quad (3.10)$$

$$B \left[\frac{-K_{xx}\phi_y^2 + 2K_{xy}\phi_x\phi_y - K_{yy}\phi_x^2}{\phi_x^2 + \phi_y^2} + K(K_y(n_x + n_y) - K_x(n_y - n_x)) \right] + K J_s^{\nabla K_s}$$

3. Solve the electrical problem, find electrically induced surface flux J_s^E from (2.6). As pointed out above, the discontinuous distributions of electrical quantities are smoothed across the surface profile - by a hyperbolic tangent law:

$$r = \frac{r_{out} + r_{in}}{2} + \frac{r_{out} - r_{in}}{2} \tanh \beta \phi(x, y) \quad (3.11)$$

where β is a large constant adjusting parameter, and r is either the electric intensity $E(x, y)$ (first electrical model), or the specific conductivity $k(x, y)$ (second electrical model)

4. Given values of the electrical intensity E along the GBs, calculate electrically induced GB fluxes, J_{gb} , from (2.12). Applying boundary condition (2.14), calculate corrected values of J_s^E along grid lines $x = 0, x = L$
5. Calculate the second term in (3.4) by applying the formula (2.2) where J_s^E replaces K_s .

4 Numerical results and discussion

Several comments should be made before we present the results of the numerical simulations.

- Due to the large number of material parameters involved we concentrate on the influence of the one which was predicted to greatly affect the grooving process, i.e. the ratio of the GB to surface diffusivity, $r_d = D_{gb}/D_s$ [1]. The parameter set we choose for the simulations corresponds to copper, Cu , at temperatures about 600 K. It should be noted that (i) the experimentally measured values of diffusivities could vary, according to different sources, by up to 3 orders of magnitude, and (ii) D_s can be smaller than D_{gb} , due to, for example, surface contamination, thus giving $r_d > 1$. Accordingly, we fix the value of D_s and vary D_{gb} in a wide range, thus varying the GB flux J_{gb} (2.12).
- We study the advancing (elongating) grooves characterized by the positive values of J_{gb} (matter flows out of the groove cavity and into the GB). In this case the electric field intensity vector is directed upwards (see Fig. 1), the positive potential being prescribed on the lower boundary of the computational box and the negative potential on the upper one. Reversing the direction of the field produces receding grooves or “ridges”, Fig. 8, characterized by a negative GB flux (matter flows out of the GB into the groove cavity). The advancing grooves are of more practical interest, as explained in the Introduction.
- Most of our results are obtained with electrical model 2 (see section 2.1), based on the solution of Laplace’s equation for the potential. As expected, this model produced more accurate results than the approximate model 1 based on the piecewise-constant electrical field. However, model 1¹ proved to be rather useful in our simulations, since it produced qualitatively good results in greatly reduced (comparable to the model 2) computational times; for very fine grids (80×80 resolution) the speedup achieved is by as much as a factor of 6.

Fig. 4 (a)-(d) shows the space/time evolution of the initially flat surface of the conductor for different values of r_d . The parameters are as in Figs. 2, 3 and $U^+ = -U^- = 5.0 \times 10^{-3} V$, $k_{in} = 10^8 (\Omega m)^{-1}$, $k_{out} = 10^7 (\Omega m)^{-1}$, $\delta_{gb} = \delta_s = 3.5 \times 10^{-10} m$, $z_s^* = z_{gb}^* = 5$. The surface profiles are dumped every 5000 time steps, the dimensions of the computational box are $0.5 \mu m \times 0.5 \mu m$, and the grid has a 60×60 resolution.

¹Or even more simplified model of the constant field throughout the entire domain $C + O$ (Fig. 1) used in most, if not all studies of electromigration (see [3] for example)

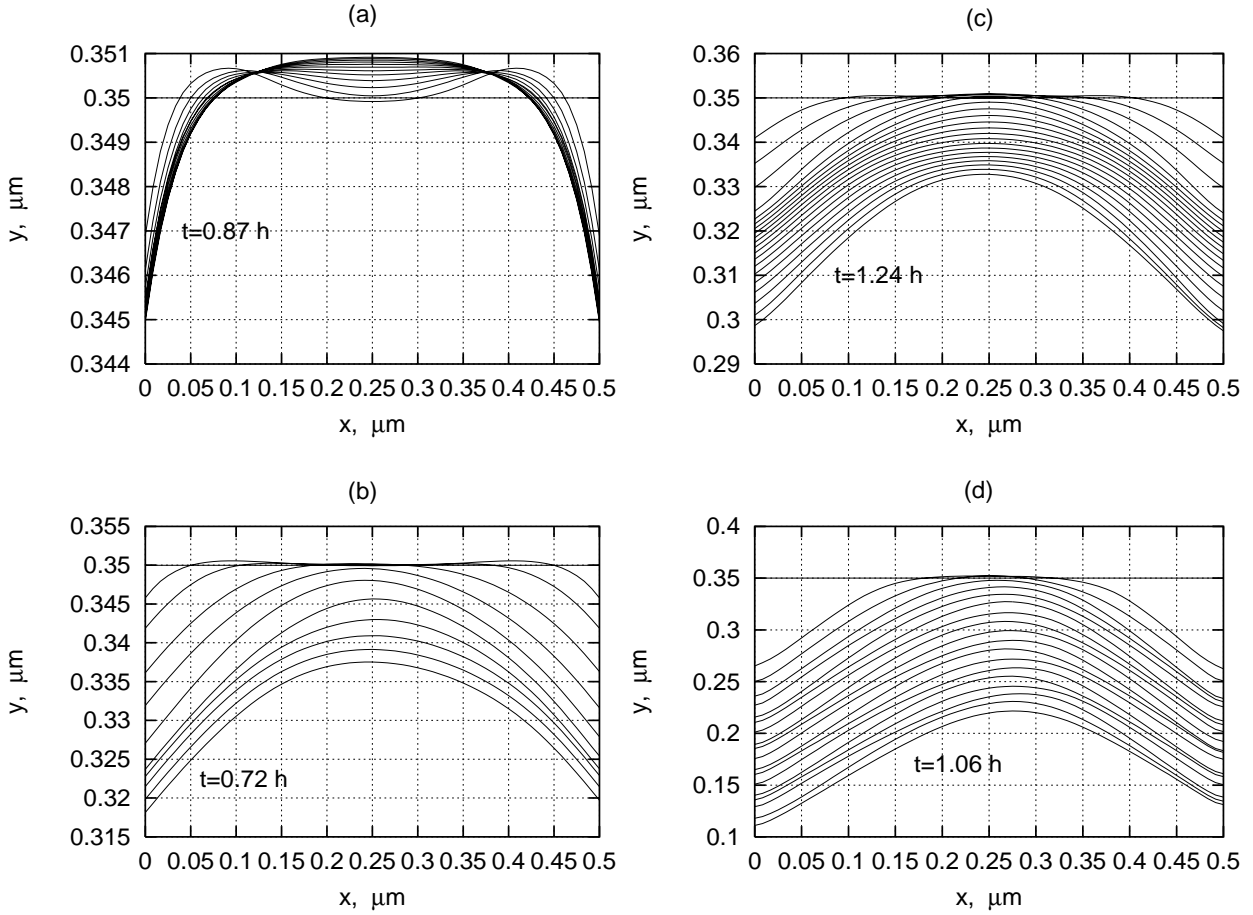


Figure 4: GB grooving by surface/GB diffusion driven by the surface curvature gradients and the electromigration. (a): $r_d = 0.224$, (b): $r_d = 0.336$, (c): $r_d = 0.561$, (d): $r_d = 22.424$. The surface profiles are dumped every 5000 time steps. The time labels correspond to the (physical) time at which the last profile is dumped.

In case r_d is much less than one (Fig. 4 (a)), i.e. the GB flux is relatively small, and we observe that the evolution of the surface is similar to the one shown in Fig. 3. It slows down in time, providing to be not very dangerous in the sense of failure of the conductor. The evolution proceeds faster as r_d increases (Fig. 4 (b)). After the GB grooves merge and form a single profile, this profile starts to advance slowly (note that the surface curvatures at the groove roots are still positive, at least during the time of the observation). Yet larger values of r_d (Fig. 4 (c)) result in changes of the morphology of the surface profile in the near-groove-tip regions. The latter means that the sign of the surface curvatures at the groove tips changes from being positive to a negative one in a relatively short time after the evolution starts, indicating the surface tendency to form so-called slits. In the case of Fig. 4 (c) this transition takes place at the time step n^* , $15000 < n^* < 20000$; see also Figures 6, 7. No qualitative change in the surface shapes is observed as r_d is further increased - up to the limit where the numerical method is applicable (note the significant losses of accuracy in Fig. 4 (d), which corresponds to $r_d = 22.424$). Fig. 4 (d) differs from Fig. 4 (c) only in the

increased velocity of the surface's advance and in a more rapid transition from positive to negative curvature at the groove roots (the decreased n^*). The evolution regime shown in Fig. 4 (c), (d) is known as the *A*-regime [1, 2].

In Fig. 5 (a) - (d) we plot the distance d traveled by the groove tip as a function of time. Fig. 5 (a) corresponds to the case of Fig. 4 (d) ($r_d = 22.424$, $L = 0.5 \mu m$, $U = U^+ = U^- = 5.0 \times 10^{-3} V$). One sees that the steady-state velocity of the surface advance is attained rather rapidly, within approximately 6 min. Also note that the groove tip traveled (in only 1 hour) a distance which is a little less than half the grain size. In Fig. 5 (b), (c) we investigate the influence of the grain size, L . When r_d is small and the applied voltage is small too (Fig. 5 (b), $r_d = 2.424$, $U = 1.0 \times 10^{-4} V$), the evolution is driven mostly by the surface flux $J_s^{\nabla K}$. Then, smaller sizes of the grains result in larger velocities of the groove tip. This is because the curvature of the surface increases as the grain size decreases, resulting in the increase of $J_s^{\nabla K}$. The example of such a transitive grooving regime (from classical Mullins regime, Fig. 4 (a) to *A*-regime, Fig. 4 (c), (d)) is presented in Fig. 4 (b). If electrically induced fluxes J_s^E

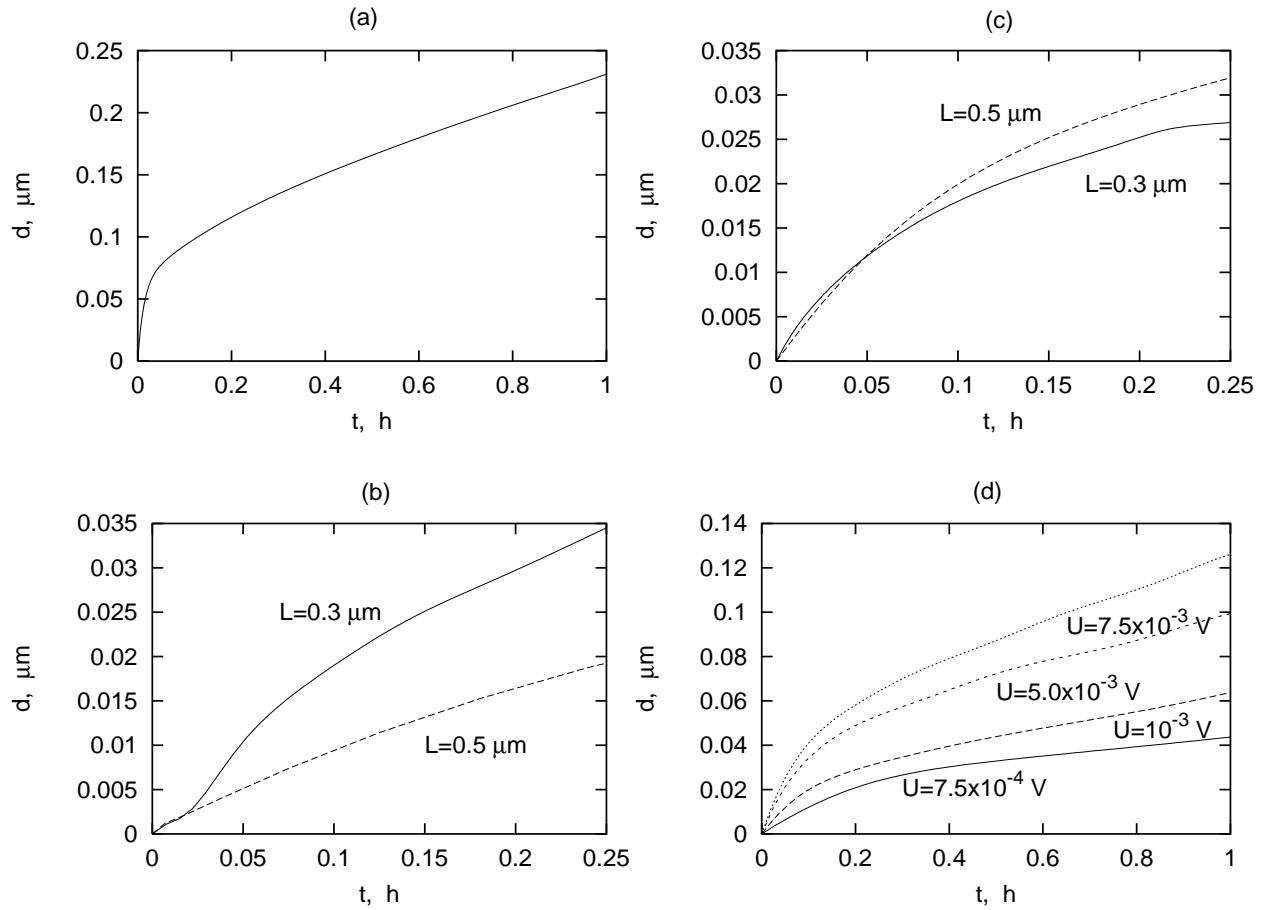


Figure 5: Distance d traveled by the groove tips as a function of time. (a): $r_d = 22.424$, refer to Fig. 4 (d); (b): $r_d = 2.424$, $U = 1.0 \times 10^{-4} V$; (c): $r_d = 2.424$, $U = 1.0 \times 10^{-3} V$; (d): $r_d = 2.424$, $L = 0.5 \mu m$.

and J_{gb} are dominant (*A*-regime, Fig. 5 (c), $r_d = 2.424$, $U = 1.0 \times 10^{-3} V$) then, in

contrast with the previous case, larger grain sizes result in larger groove tip velocities, as predicted in [2]. The dependence of the groove tip velocity on the applied voltage is illustrated by Fig. 5 (d) ($r_d = 2.424$, $L = 0.5 \mu\text{m}$). GB grooving proceeds faster in strong electric fields due to the amplification of the electromigration and associated diffusion fluxes J_s^E and J_{gb} .

For completeness, in Fig. 6 (a)-(d) and in Fig. 7 (a)-(d) we present plots of the surface curvature, the $J_s^{\nabla K}$ and J_s^E diffusion fluxes, and the normal velocity function F for the case of Fig. 4 (c). The data in Fig. 6 correspond to time step 1000 (transient stage), while the data in Fig. 7 correspond to time step 35000 (steady-state stage). Grooves develop faster during the transient stage (compare Fig. 6 (d) and Fig. 7 (d), see also Fig. 5), when the curvature of the surface in the near-groove tips regions is positive and both $J_s^{\nabla K} > 0$ and $J_s^E > 0$ fluxes tend to elongate the grooves, providing the flow of matter out of the groove tips. As the steady-state approaches, the curvature of the surface in the near-groove tips regions becomes negative (Fig. 7 (a)) and the J_s^E flux is still into the GB but the flux $J_s^{\nabla K}$ changes the direction and slows the evolution down (Fig. 7 (b), (c)).

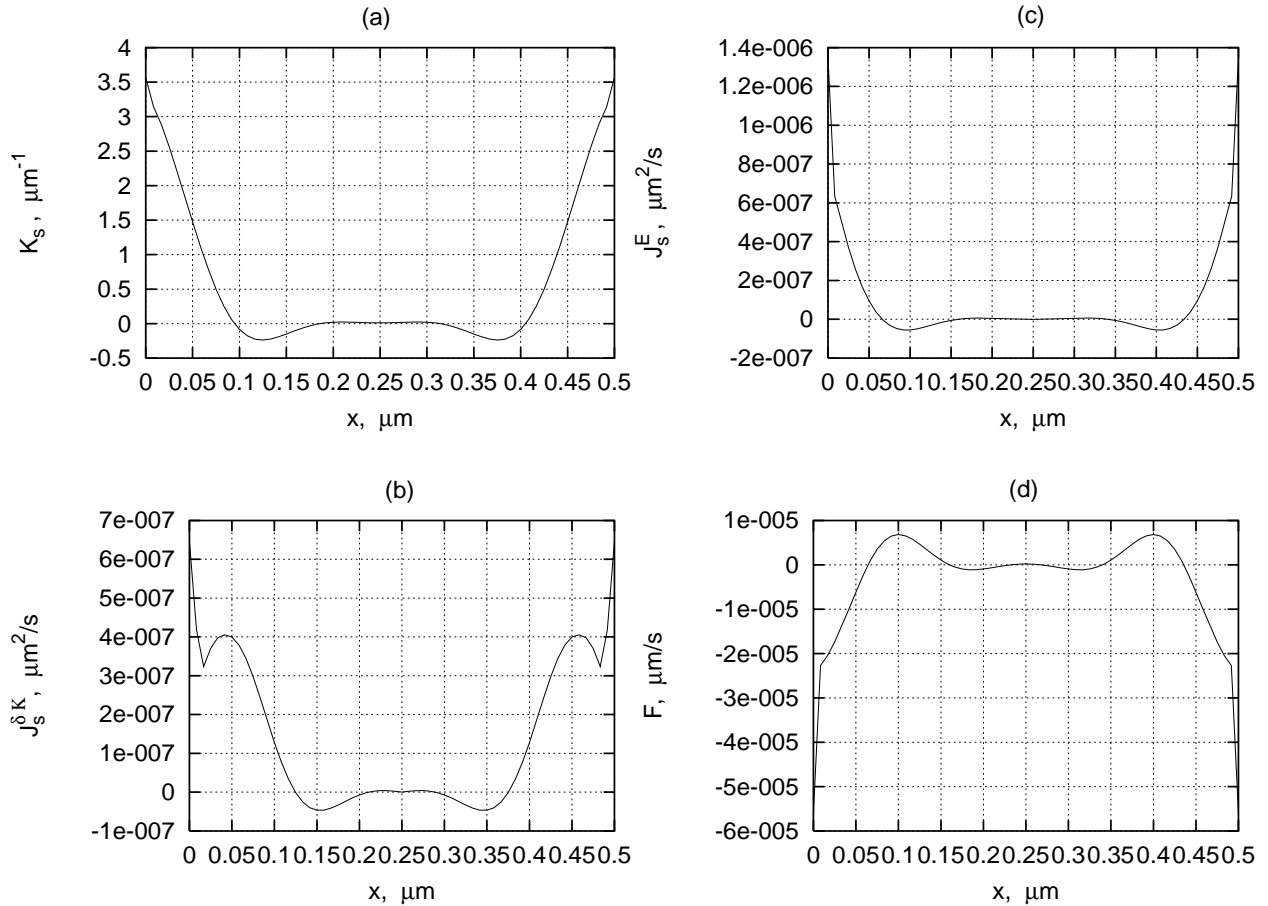


Figure 6: Plots of the surface's curvature (a), diffusion fluxes (b), (c) and the normal velocity function (d). $r_d = 0.561$, refer to Fig. 4 (c). The corresponding time step is 1000.

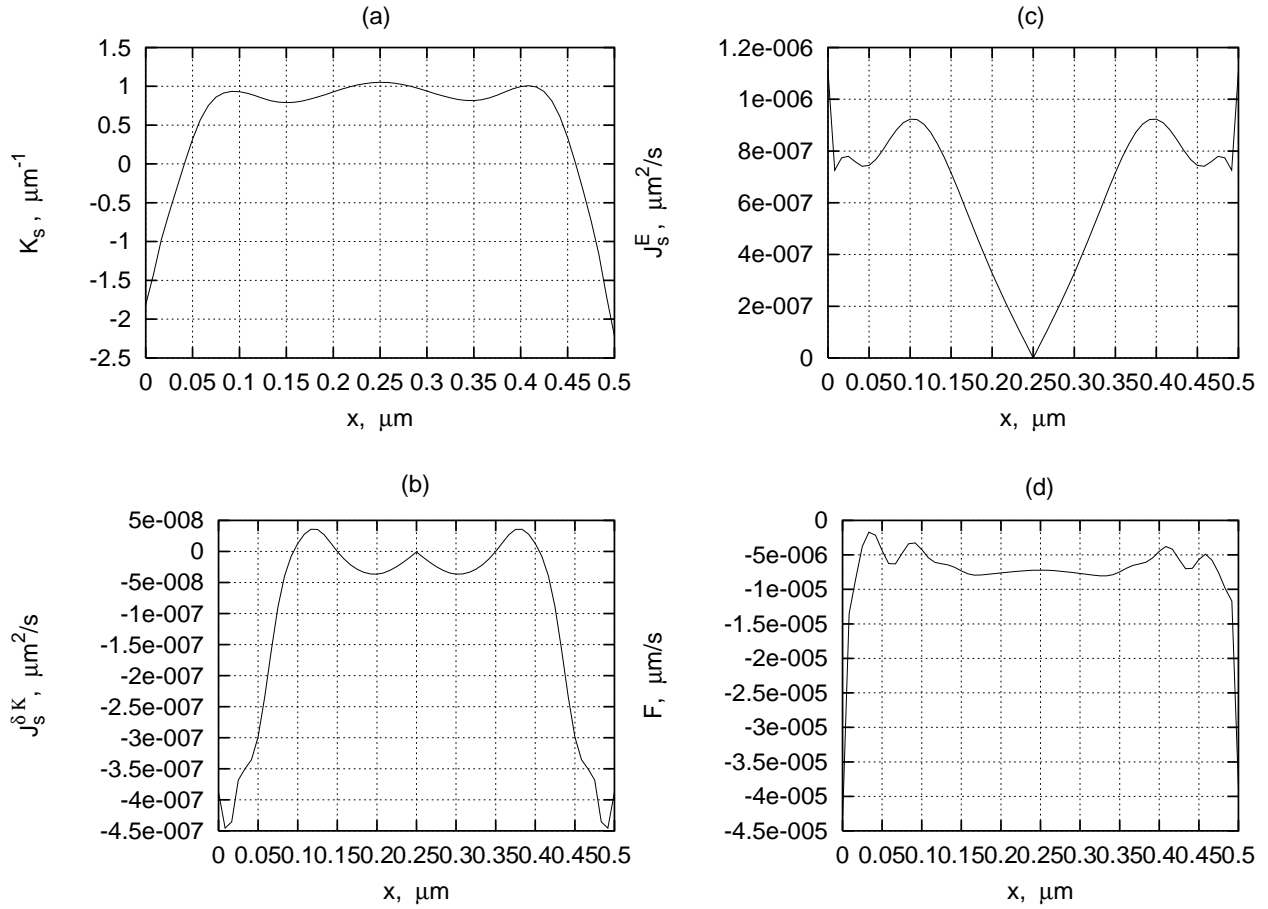


Figure 7: Same as Fig. 6, but the data correspond to the time step 35000 at Fig. 4 (c).

Fig. 9 shows the *A*-regime of GB grooving obtained with the use of the electrical model 1 (see section 2.1; to be compared with the Fig. 4 (d)). The computations are less accurate if this model is employed, resulting in highly asymmetric surface profiles. However, the dynamics of surface evolution could be predicted from these simulations and we made a heavy use of the electrical model 1 for trial numerical experiments. It is worth to note that the run time to obtain Fig. 9 is 2.2 hours on SGI workstation with 194 MHz IP25 processor, compared to 8.1 hours for Fig. 4 (d).

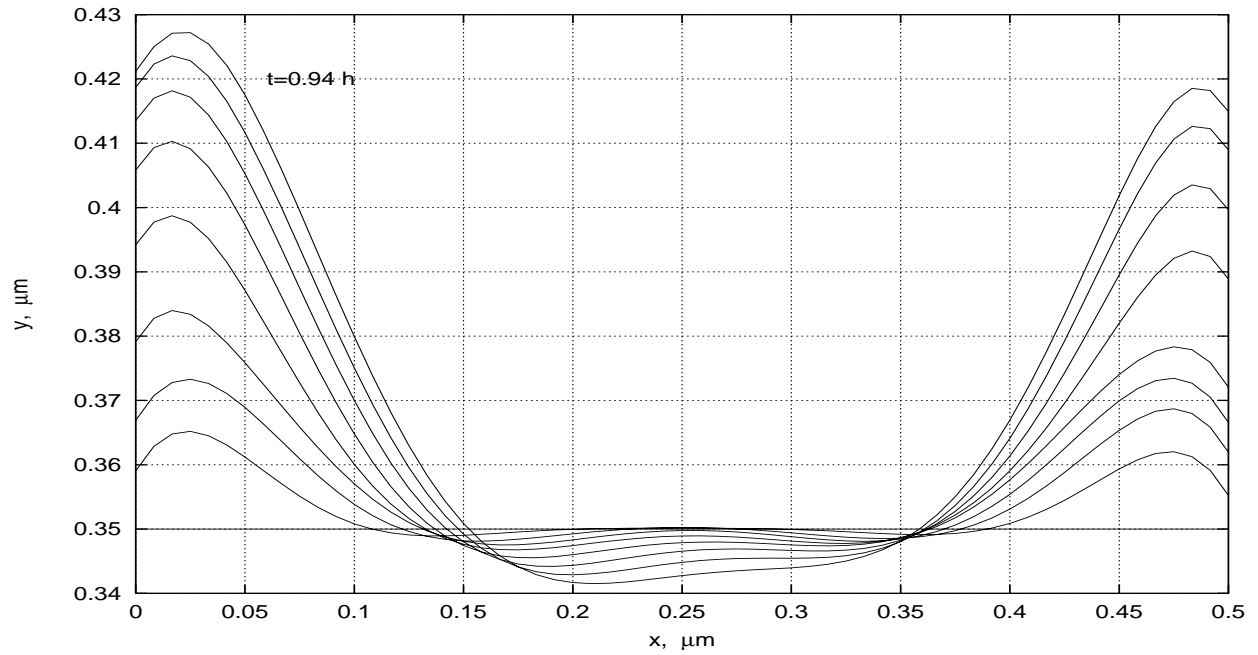


Figure 8: The ridges formed if the matter flows into the groove tips ($r_d = 1.121$, the electric field intensity vector is directed from top to bottom). The physical parameters are as in Fig. 4.

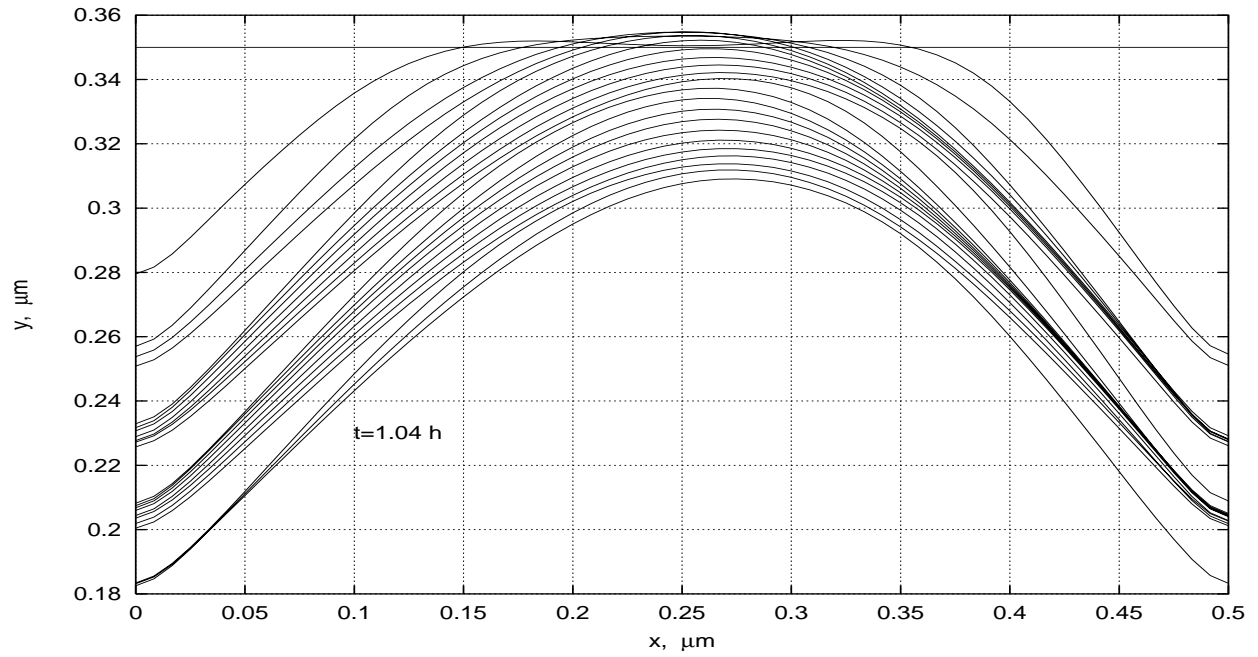


Figure 9: GB grooving, $r_d = 22.424$ (compare to Fig. 4 (d)). The electrical model 1 was used.

5 Conclusions

The Level Set method was used to model the GB grooving by surface/GB diffusion in an idealized polycrystalline interconnect. The diffusion is driven by surface curvature gradients and external applied electric field. The results demonstrate the high potential of the LS method for the simulation of complex failure phenomena in microelectronic interconnects. The plans for future research are:

- to obtain more physical results with the current version of the code and compare them to experimental ones
- to improve our numerical procedure to make possible the simulation of the propagation of slits (*B*-regime, [1, 2, 3]). The latter are characterized by (almost) straight vertical walls ² and negative curvatures at the slit tips. The slits are formed at high values of r_d , and are supposed to propagate in a *local* steady state, leaving the rest of the surface behind. Physically, the surface of the conductor cannot accomodate a very large GB flux; the groove tips then become diffusively detached from the remaining surface. At the moment our numerical procedure does not allow to fully trace the evolution of the slits and the surface left behind. In our opinion, a locally refined grid is needed to provide high accuracy in the near-slit-tip regions; however, the adaptation of the LS method to such grids may be not straightforward. In our simulations (which make use of an uniform grid), the instability steps in shortly.
- to incorporate mechanical stress in the analysis
- to speed up the computations by making use of an implicit scheme for the solution of the equation (3.1). This will allow larger time steps.

6 Appendix

Derivation of the 2-dimensional electrostatic equation

We consider a conducting strip made of a thin metal film, attached to a strip of nonzero conductivity substrate. The metal film may be continuous or it may be made of conducting patches with voids in between. We allow the metal film and substrate to have variable thickness. In the present formulation we neglect the interface resistance. The electrodes are attached to the strip and to the substrate. We may want to compute the local field strength which determines the resulting electromigration. This is a more realistic model then the model based on the assumption of a zero conductivity substrate. It allows us also to consider the behaviour of a metal film with varying effective thickness at no extra cost.

6.1 The 3-dimensional problem

The 3-dimensional Problem Ohm's law implies: $\vec{j} = \sigma \vec{E} = -\sigma \nabla_3 \phi$, where \vec{j} is the electric current density vector, \vec{E} is the electric field vector, ϕ is the electric potential

²The flux $J_s^{\nabla K}$ is zero along these walls.

and σ is the material conductivity. For steady fields Maxwell's equations with vanishing space charge give:

$$\nabla_3 \cdot \vec{j} = 0, \text{ where } \nabla_3 = \left(\frac{\partial}{\partial x}, \frac{\partial}{\partial y}, \frac{\partial}{\partial z} \right). \quad (6.1)$$

Hence

$$\nabla_3 \cdot (\sigma \nabla_3 \phi) = 0. \quad (6.2)$$

At all external (lateral) boundaries there is no flux in the direction of the normal, \vec{n} , so that $\vec{n} \cdot \vec{j} = 0$, and using (6.1) one gets:

$$\vec{n} \cdot \nabla_3 \phi = 0. \quad (6.3)$$

The conditions (6.3), together with values of the potential specified at the strip and substrate edges and the continuity and jump conditions at the interface, constitute boundary conditions for equation (6.2) in the two layers. Thus the three dimensional potential can be found, in principle, as the solution of a well-posed three-dimensional boundary value problem. However such a solution can be very expensive to get in the present geometry, in particular as singularities in the solution will appear at sharp geometrical corners at crystal boundaries or voids, requiring high resolution or complicated integration formulae. To avoid this (probably unrealistic) behaviour of the solution and to avoid solving three dimensional problems many times, as required by the time development of the process, we proceed with an approximate approach suggested by (singular) perturbation theory.

6.2 The 2-dimensional equation

We assume that ϕ and σ change over a characteristic length scale L in the horizontal directions x and y but over a scale H in the vertical. Furthermore we assume that $\epsilon = H/L \ll 1$. Using scaled variables in (6.2),

$$(X, Y, Z) = (x/L, y/L, z/H) \quad (6.4)$$

we get:

$$\epsilon^2 \nabla_2 (\sigma \nabla_2 \phi) + \frac{\partial}{\partial Z} \left(\sigma \frac{\partial \phi}{\partial Z} \right) = 0, \text{ where } \nabla_2 = \left(\frac{\partial}{\partial X}, \frac{\partial}{\partial Y} \right). \quad (6.5)$$

Singular perturbation analysis considers an expansion

$$\phi = \phi_0 + \epsilon^2 \phi_1 + \epsilon^4 \phi_2 + \dots \quad (6.6)$$

where ϕ_k are functions of order $O(1)$ in ϵ . Substitution of (6.6) in (6.5) gives relations for the functions ϕ_k by grouping terms according to their order in ϵ and equating each group to zero. The zeroth order term gives : $\partial^2 \phi_0 / \partial Z^2 = 0$, thus ϕ_0 is a linear function in z for every x and y while taking into account (6.3) kills off the z dependence, so that:

$$\phi_0 = \phi_0(X, Y). \quad (6.7)$$

Thus at this stage ϕ_0 is an arbitrary function of the horizontal coordinates X and Y . The first order equation and the boundary conditions in Z result ultimately in the approximate two-dimensional equation for ϕ_0 [10]:

$$\nabla_2 (h_1 \sigma_1 + h_2 \sigma_2) \nabla_2 \phi_0 = 0 \quad (6.8)$$

where h_1, σ_1 and h_2, σ_2 are, respectively, the heights and conductivities of the two layers under consideration. The equation (6.8) is solved with boundary conditions in the (X, Y) plane. We remark that the approximate independence of the potential ϕ on the Z coordinate justifies also the two dimensional approach for the electromigration equation. This behaviour is a consequence of the small aspect ratio assumption and the normal derivative boundary conditions (6.3), where one must also involve a small slope assumption.

References

- [1] E. Glickman, M. Nathan, *J. Appl. Phys.* **80**, 3782, (1996).
- [2] L. Klinger, E. Glickman, V. Fradkov, W. Mullins, and C. Bauer, *J. Appl. Phys.* **78**(6), 3833-3838, (1995).
- [3] L. Klinger, X. Chu, W. Mullins, and C. Bauer, *J. Appl. Phys.* **80**(12), 6670-6676, (1996).
- [4] W.W. Mullins, *J. Appl. Phys.* **28**, 3, 333-339, (1957).
- [5] M. Khenner, A. Averbuch, M. Israeli, M. Nathan, submitted.
- [6] S.A. Hackney, *Scripta Metall.* **22**, 1731, (1988).
- [7] I.A. Blech, C. Herring, *Appl. Phys. Lett.* **29**, 131, (1976).
- [8] J. Herring, *Appl. Phys.* **21**, 301, 1950.
- [9] W.W. Mullins: in *Metal Surfaces: Structure, Energetics and Kinetics*, ASM, Metals Park, OH, p. 17, 1963.
- [10] A. Averbuch, M. Israeli, I. Ravve, submitted.
- [11] J.A. Sethian, Level Set methods and fast marching methods: evolving interfaces in computational geometry, fluid mechanics, computer vision and materials science, *Cambridge University Press*, 1999.
- [12] S. Osher, C.W. Shu, *J. Numer. Anal.* **28**, 907-922, (1991).
- [13] C.-W. Shu, S. Osher, *J. Comput. Phys.* **77**, 439-471, (1988).
- [14] H.-K. Zhao, T. Chan, B. Merriman, S. Osher, *J. Comput. Phys.* **127**, 179-195, (1996).
- [15] M. Sussman, P. Smereka, S. Osher, *J. Comput. Phys.* **114**, 146-159, (1994).
- [16] W.W. Mullins, *Metall. and Materials Trans.* **26A**, 1917-1929, (1995).